Molecular Imaging of Changes in the Prevalence of Vascular Endothelial Growth Factor Receptor in Sunitinib-Treated Murine Mammary Tumors

Zoia Levashova[1], Marina Backer[2], Carl V. Hamby[3], John Pizzonia[4], Joseph M. Backer[2], and Francis G. Blankenberg[1]

[1]Department of Radiology/MIPS, Stanford University, Palo Alto, California; [2]Sibtech, Inc., Brookfield, Connecticut; [3]Department of Immunology and Microbiology, New York Medical College, Valhalla, New York; and [4]FUJIFILM Medical Systems USA, Inc., Woodbridge, Connecticut

Several drugs targeting vascular endothelial growth factor (VEGF) and its receptors (VEGFRs) are approved for cancer treatment. However, these drugs induce relatively modest and frequently unpredictable tumor responses. In this work, we explored whether noninvasive imaging of VEGFR, a direct target of antiangiogenic drugs, can provide real-time information on responses to the treatment with sunitinib, a small-molecule VEGFR inhibitor approved by the Food and Drug Administration. **Methods:** We imaged VEGFR in an orthotopic mammary tumor model during the course of treatment with sunitinib using a recently developed SPECT tracer, a ^{99m}Tc-labeled single-chain VEGF (scVEGF), that binds to and is internalized by VEGFR. Tumors from imaged mice were harvested and cryosectioned, and alternating sections were analyzed by autoradiography and immunohistochemistry to determine the expression of endothelial cell markers VEGFR-2 and CD31. **Results:** In vitro assays with endothelial cells overexpressing VEGFR-2 established that sunitinib does not inhibit VEGFR-2–mediated uptake of scVEGF-based tracers. SPECT and autoradiography with ^{99m}Tc-scVEGF of tumor cryosections revealed a 2.2- to 2.6-fold decrease in tracer uptake after 4 daily doses of sunitinib. However, once treatment was discontinued, tracer uptake rapidly (3 d) increased, particularly at the tumor edges. Immunohistochemical analysis of VEGFR-2 and CD31 supported SPECT and autoradiographic imaging findings, revealing the corresponding depletion of VEGFR-2– and CD31-positive endothelial cells from tumor vasculature during therapy and the rapid reemergence of VEGFR-2– and CD31-positive vasculature at the tumor edges after discontinuation of treatment. **Conclusion:** Our findings suggest that imaging with ^{99m}Tc-scVEGF might be useful for monitoring VEGFR responses to antiangiogenic treatment regimens.

Key Words: VEGF receptors; SPECT; imaging; sunitinib; ^{99m}Tc-scVEGF

J Nucl Med 2010; 51:959–966
DOI: 10.2967/jnumed.109.072199

Received Oct. 30, 2009; revision accepted Feb. 19, 2010.
For correspondence or reprints contact: Francis G. Blankenberg, Lucile Salter Packard Children's Hospital at Stanford, 725 Welch Rd., Rm. #1673, Stanford, CA 94304-1601.
E-mail: blankenb@stanford.edu

Vascular endothelial growth factor (VEGF) signaling is required for the development and maintenance of new blood vessels that enable the continued growth of primary tumors and metastatic lesions. Because of its critical role, VEGF signaling is a major target for new anticancer therapies. Several drugs targeting VEGF and its receptors (VEGFRs) are already approved for use as single agents or as part of combination therapy for treatment of common solid tumors, including breast, colon, and renal cancer (*1,2*). There are also multiple late-stage clinical trials for Food and Drug Administration–approved and experimental drugs targeting VEGF and VEGFR for all major cancers. However, individual responses to these drugs or regimens are unpredictable, being effective in only relatively small subsets of patients, and can have serious side effects (*1–7*).

Currently, the mechanisms of action of VEGF- and VEGFR-targeted drugs, and modes of resistance in vivo, are not fully characterized or well understood (*5–7*). Judging by immunohistochemical analyses, dynamic contrast-enhanced MRI, and ultrasound imaging, the overall outcome of existing VEGF- and VEGFR-targeted drugs appears to be the transient regression of tumor vasculature, followed by an adaptive, hypoxia-induced revascularization, which is accentuated by abrupt interruption or cessation of therapy. Both these phases depend on the complex interplay of local and systemic processes, which are, most likely, affected by the sensitivity of not only VEGFR but also other tyrosine kinase receptors to existing VEGFR-inhibiting anticancer drugs. Nevertheless, it is reasonable to expect that the prevalence and activity of the immediate drug target, VEGFR expressed on tumor endothelial cells, can strongly influence or even determine the dynamics and the overall outcome of these processes. Therefore, there is a need for noninvasive imaging methods that can assess VEGFR expression during the course of antiangiogenic treatment (*8*). Such information could be

used to design and monitor treatment regimens that would prolong tumor vasculature regression and prevent revascularization.

We have recently developed a family of tracers based on an engineered single-chain VEGF (scVEGF) composed of 2 fused 3-112 amino acid fragments of $VEGF_{121}$ and an *N*-terminal 15–amino acid Cys-tag containing a unique cysteine residue for site-specific attachment of various payloads (*9*), including ^{99m}Tc for SPECT (*10*). scVEGF-based tracers bind to VEGFR with the same affinity as parental VEGF (*9,10*) and are internalized by VEGFR, providing information on the prevalence of functionally active receptors. Because VEGFRs are expressed in tumor vasculature at higher levels than in quiescent host vasculature, scVEGF-based tracers selectively and specifically accumulate within the blood vessels of tumors (*9,10*).

In the current study, we used SPECT with one such tracer, ^{99m}Tc-scVEGF, to characterize VEGFR responses to treatment with the selective VEGFR inhibitor, sunitinib (*11*), in a mouse orthotopic mammary tumor xenograft model. In addition to VEGFR, sunitinib targets receptors for platelet-derived growth factor, as well as KIT, RET, colony-stimulating factor 1 receptor, and FLT3. Sunitinib is currently approved for the treatment of advanced renal cell carcinoma and imatinib-resistant gastrointestinal stromal tumors. It is also being evaluated in more than 50 phase III clinical trials for most major types of malignant tumors, and therefore, optimization of sunitinib treatment regimens could have a significant national impact on the clinical management of cancer. We report here that SPECT with ^{99m}Tc-scVEGF reveals a complex set of changes in VEGFR prevalence in response to sunitinib treatment and that imaging data directly reflect the degree of VEGFR expression as seen by immunohistochemical analyses.

MATERIALS AND METHODS

Cell Lines and Tumor Models

MDA-231/luc tumor cells (SibTech), a luciferase-expressing derivative of MDA-MB-231 human breast carcinoma; PAE/KDR cells expressing approximately 2×10^5 VEGFR-2/cells (SibTech); and parental PAE cells (a generous gift of late Dr. Bruce Terman) were maintained in Dulbecco's modified Eagle's medium (Invitrogen) supplemented with 10% fetal bovine serum (HyClone) and 2 mM L-glutamine (Invitrogen). MDA-231/luc and PAE/KDR were authenticated at the American Type Culture Collection Molecular Authentication Resource Center on July 20, 2009. The protocols for all animal studies were approved by the Stanford University Institutional Animal Care and Use Committee. The orthotopic MDA-231/luc model of xenogeneic breast cancer was established as described (*9,10,12*). Briefly, we injected $1.5–2 \times 10^6$ MDA-231/luc tumor cells into the left axillary fat pad of 5- to 8-wk-old adult male severe combined immunodeficiency disease/Ncr (BALB/c background) mice (Taconic). Animals with tumors ranging between 200 and 500 mm^3 (17–24 d after cell inoculation) were randomized into study groups. Treated animals received sunitinib (LC Laboratories) prepared as previously described (*11*), via gavage feeding, 80 mg/kg per day.

Tracers for Fluorescent Microscopy

scVEGF/Cy is produced in SibTech. The plasmid DNA–encoding scVEGF(2GA) mutant, scVEGF with the G107A and G218A amino acid substitutions, was generated by GeneWiz. The resulting mutant scVEGF(2GA) was produced at SibTech. For site-specific modification with the fluorescent dye AlexaFluor594-C_5-maleimide (Invitrogen), scVEGF or scVEGF(2GA) was deprotected as described elsewhere (*9,10*); incubated with 2 molar equivalents of AlexaFluor 594-C_5-maleimide for 1 h at room temperature in 0.1 M Tris-HCl and 1 mM ethylenediaminetetraacetic acid, pH 8.0; and purified by reversed-phase high-performance liquid chromatography on a Vydac Protein C4 300 Å 5-μm column (Grace Davison Discovery Sciences) using a gradient of acetonitrile in aqueous 0.1% trifluoroacetic acid. The purified conjugates were lyophilized and reconstituted in 50 mM Tris-HCl, pH 8. Functional activity of the resulting fluorescent tracers was tested as previously described (*9,10*).

In Vitro Cellular Uptake of scVEGF-Based Tracers

For quantitative uptake experiments, PAE/KDR and PAE cells were plated in black clear-bottom 96-well plates (BD Falcon), 20,000 cells per well. Twenty hours later, cells were shifted to fresh culture medium, with or without 1 μM sunitinib, and incubated for 1 h in a CO_2 incubator. For dose-dependence, varying scVEGF/Cy was added to cells in triplicate wells and incubated for 20 min under normal tissue culture conditions. For kinetics, 5 nM scVEGF/Cy was added to cells for varying times. Then the medium was removed, and the cells were washed extensively with phosphate-buffered saline and then with phosphate-buffered saline containing 0.5 M NaCl, fixed in fresh 4% ultrapure methanol-free formaldehyde (Polysciences), air-dried, and imaged in a Starion FLA-9000 device (Fujifilm Medical Systems USA). For fluorescent microscopy, cells were plated in 8-well chamber slides, preincubated for 1 h 20 h later with or without 1 μM sunitinib, and exposed to 5 nM scVEGF/Al594. Cells were washed and fixed in the same manner as for the kinetics, mounted in mounting medium for fluorescence with 4′,6-diamidino-2-phenylindole for nuclear counterstaining (Vector Labs), and observed in an AxioObserver microscope (Zeiss) using ×40 oil objective. For neutralization assays, a 2- to 5-fold molar excess of bevacizumab (Avastin; Genentech) or control human IgG (Sigma) was added to the fluorescent tracers scVEGF/Al594 or scVEGF(2GA)/Al594 in complete culture medium, incubated for 1 h at room temperature, and then added to PAE/KDR cells to a final scVEGF concentration of 5 nM. After a 20-min incubation, cells were washed, fixed, and mounted as described for kinetics.

Preparation of Radiolabeled ^{99m}Tc-scVEGF

scVEGF (SibTech) was deprotected and radiolabeled, using ^{99m}Tc-tricine as a precursor complex as described previously (*10*), yielding ^{99m}Tc-scVEGF tracers that are stable in circulation. Briefly, lyophilized tin-tricine reagent was reconstituted with 1.0 mL of degassed saline to give a final $SnCl_2 \cdot 2H_2O$ concentration of 0.6 mg/mL and a final tricine concentration of 20 mg/mL (pH 7.1). Tin-tricine (10 μL) was added to 30–50 μg of premixed deprotected scVEGF and 370–555 MBq (10−15 mCi) of ^{99m}Tc-pertechnetate in a final volume of 50–100 μL. After 30 min of incubation at 37°C, radiolabeled protein, named ^{99m}Tc-scVEGF, was purified by gel filtration on PD-10 Sephadex-25 columns (GE Healthcare). Specific activities ranged from 4.8 to 7.4 MBq/μg (130–200 μCi/μg) of protein, with a radiopurity of approximately

95%, as determined by instant thin-layer chromatography using phosphate-buffered saline as a solvent.

SPECT and Autoradiography

For SPECT, 74–148 MBq (2–4 mCi) of ^{99m}Tc-scVEGF per mouse was injected via the tail vein. SPECT images were obtained at 1 h after injection using a small-animal SPECT γ-camera (A-SPECT, LumaGEM; Gamma Medica) with the following parameters: 360° rotation, 64 steps, 30 s per step, 0.5-mm pinhole aperture, 64 × 64 image matrix, and a 2.7-cm field of view. For autoradiography, tumors and pectoral muscle (from the contralateral chest wall) were snap-frozen immediately after imaging, cryosectioned (60-μm thickness), and exposed to a phosphor storage screen for 16 h. The phosphor screen images were read out with a laser digitizer at a pixel dimension of 50 μm. Region-of-interest analysis of radiotracer activity was performed using ImageQuant TL software (GE Healthcare) with 4 rectangular areas per tumor rim, center, and contralateral pectoral muscle. The maximal counts per pixel of the rim and the average counts per pixel of the center of the tumor were normalized to corresponding contralateral pectoral muscle uptake (minimum background counts per pixel). The uptake of the rim (maximum) and center of each tumor were then divided by the contralateral pectoral muscle uptake and presented as rim-to-background and center-to-background ratios, respectively.

Immunohistochemical Staining

Tumor cryosections (thickness, 20 μm) were stained for VEGFR-2 (Flk-1, rat monoclonal antibody; BD Pharmingen) and CD31 (PECAM, rat monoclonal antibody; BD Pharmingen). Apoptosis was assessed by terminal deoxynucleotidyl transferase-mediated dUTP nick-end labeling (TUNEL) (Apo-BrdU-IHC In Situ DNA Fragmentation Assay Kit; BioVision) according to the manufacturer's instructions. Immune complexes were visualized by chromogenic assay using Vectastatin Elite ABC Kit (Vector Labs) and VIP Substrate Purple Kit (Vector Labs). For quantitative analysis, color images were acquired with ×4 objective, exported into Adobe Photoshop, and converted into gray-scale images, and a threshold to the same dynamic range was applied. The percentage of black pixels corresponding to immunostained area was determined using histogram analysis either for the whole images or for multiple small rectangular areas that were selected to cover the whole image.

Statistical Analysis

Data that were normally distributed were compared by standard *t* tests for differences among means. Immunohistochemical data that were not normally distributed were analyzed with the nonparametric Kruskal–Wallis rank test, and the significance levels of differences between group medians were determined by applying a *Z* test with Bonferroni adjustment for multiple comparisons.

RESULTS

Sunitinib Does Not Inhibit Uptake of scVEGF-Based Tracer

Sunitinib inhibits VEGFR-2 tyrosine phosphorylation with a median effective concentration of 0.01 μM (*11*). Because conflicting reports on the role of tyrosine phosphorylation in VEGFR-2 internalization exist (*13–15*), we tested whether sunitinib could inhibit the VEGFR-2–mediated uptake of scVEGF-based fluorescent tracers by porcine aortic endothelial cells PAE/KDR expressing high levels of VEGFR-2 (*9*). Although in these cells complete inhibition of scVEGF-induced VEGFR-2 tyrosine phosphorylation was reached in the presence of 100 nM sunitinib (Supplemental Fig. 1; supplemental materials are available online only at http://jnm.snmjournals.org), we found that 1 μM sunitinib did not affect dose-dependent intracellular accumulation of scVEGF/Cy fluorescent tracer by PAE/KDR cells (Fig. 1). Although sunitinib induced a small but significant difference in kinetics of scVEGF/Cy accumulation in the first 5–10 min, this difference disappeared after 15–20 min of incubation (Supplemental Fig. 2).

To track internalized scVEGF by fluorescent microscopy, we used fluorescent scVEGF/Al594 tracer. scVEGF/Al594 was internalized by PAE/KDR cells both with and without sunitinib treatment and was readily detected in specks of increased fluorescent signal accumulated in the perinuclear area (Supplemental Fig. 3). As expected, control PAE cells did not accumulate any detectable amounts of the tracer

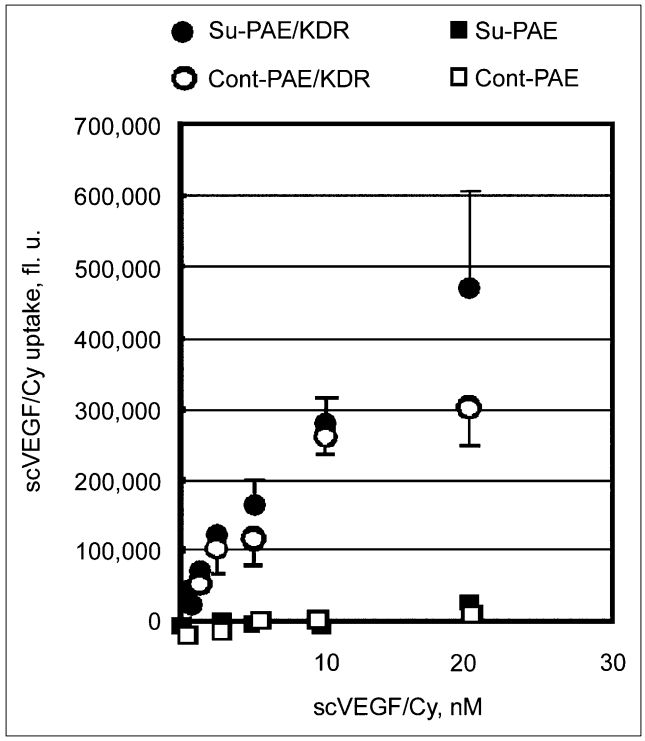

FIGURE 1. Receptor-mediated uptake of scVEGF/Cy in presence of sunitinib. After 1 h of preincubation with 1 μM sunitinib, PAE/KDR and PAE cells in triplicate wells were exposed to varying concentrations of scVEGF/Cy with 1 μM sunitinib (Su-PAE/KDR and Su-PAE). Control PAE/KDR and PAE cells preincubated without sunitinib were exposed to same concentrations of scVEGF/Cy without sunitinib (Cont-PAE/KDR and Cont-PAE). After 20 min of exposure, cells were washed, fixed, and imaged. Error bars are shown only for data in presence of sunitinib. fl. u. = fluorescent units.

(data not shown). In contrast to sunitinib, bevacizumab, a VEGF-specific antibody that prevents VEGF binding to VEGFR, completely blocked scVEGF/Al594 uptake at a 2:1 bevacizumab-to-tracer molar ratio (Supplemental Fig. 4). Notably, bevacizumab did not block the internalization of scVEGF(2GA)/Al594 (Supplemental Fig. 4). That tracer is based on a scVEGF mutant with the G107A and G218A amino acid substitutions that correspond to the G88A substitutions in each subunit of native VEGF, which completely abrogates bevacizumab binding without affecting VEGFR-2 binding (*16*).

Taken together, the results obtained with fluorescent scVEGF-based probes indicate that it is unlikely that sunitinib would directly inhibit VEGFR-mediated internalization of ^{99m}Tc-scVEGF tracer in vivo. We recently found that another inhibitor of VEGFR tyrosine kinase activity, pazopanib (*17*), does not inhibit receptor-mediated internalization of scVEGF-based tracers (*18*), supporting the notion that the use of such tracers is compatible with VEGFR inhibitory drug therapy.

Sunitinib Causes Rapid Decline in ^{99m}Tc-scVEGF Tumor Uptake

To assess early effects of sunitinib treatment, MDA-231/luc tumor–bearing mice were given sunitinib at 80 mg/kg daily for 4 d. As an inhibitory dose of sunitinib is maintained in circulation for at least 12 h after drug treatment (*11*), we allowed for a 1-d recovery after the last sunitinib dose before imaging. Treated and control mice were injected with ^{99m}Tc-scVEGF, imaged, and sacrificed; after sacrifice, tumors were harvested and sectioned for autoradiographic analyses of ^{99m}Tc-scVEGF uptake and immunohistochemical staining for VEGFR-2 and the pan-endothelial marker CD31.

In agreement with a previous report (*10*), ^{99m}Tc-scVEGF tracer readily accumulated in tumors in control, but not in sunitinib-treated, mice (Fig. 2A). Autoradiography of serial tumor sections, compared with healthy contralateral tissue, confirmed a significantly higher accumulation of ^{99m}Tc-scVEGF in the tumor area in control mice than in sunitinib-treated mice (Supplemental Fig. 5).

Sunitinib Causes Rapid Decline in VEGFR-2 and CD31-Positive Cells in Tumor Vasculature

As reported previously, of 2 main VEGFRs, only VEGFR-2 is expressed in MDA-231/luc tumors and localized to CD31-positive endothelial cells (*9*). Thus, we expected that a sunitinib-induced decrease in ^{99m}Tc-scVEGF uptake might be due to the changes in VEGFR-2 prevalence, accessibility, or internalization or recycling in tumor endothelial cells. As sunitinib and other VEGF- and VEGFR-targeting drugs are known to induce a rather rapid regression of tumor vasculature (*19–25*), we assessed the effects of sunitinib on VEGFR-2 and CD31 prevalence in tumors harvested from control and treated mice. Immunostaining revealed extensive vascularization in control tumors, with somewhat higher VEGFR-2 and CD31 density

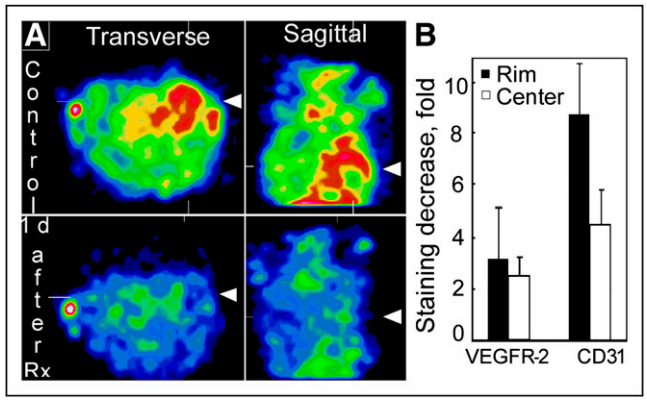

FIGURE 2. Decreased ^{99m}Tc-scVEGF tracer uptake and immunostaining for VEGFR-2 and CD31 after 4 d of sunitinib treatment and 1 d of recovery (1 d after treatment). (A) Representative SPECT images obtained with ^{99m}Tc-scVEGF tracer for treated and time-matched untreated control MDA-231/luc tumor–bearing mice. Tomographic images are from center of tumors located in left axilla and left anterior chest wall. Standard of activity (capillary tube, 1 percentage injected dose per milliliter) is seen adjacent to right axilla. Arrowheads mark location of left axillary tumor. (B) Quantitative analysis of relative decrease in VEGFR-2 and CD31 immunostaining at rim and center of tumors from treated vs. control mice. Rectangular fields (5–10) for rim and center areas on images shown in Supplemental Figure 6 were analyzed. Rx = treatment.

at the tumor edge adjacent to the underlying muscle tissue (Supplemental Fig. 6). We observed occasional small TUNEL-positive areas; however, in general, the level of apoptosis was low (Supplemental Fig. 6).

Four-day sunitinib treatment led to a significant decrease of VEGFR-2 and CD31 immunostaining throughout the tumor section, including tumor edges (Supplemental Fig. 6). Interestingly, quantitative analysis of immunostaining indicated that the magnitude of the sunitinib-induced decrease in VEGFR-2 was lower than that for CD31, both for the rim and center areas (Fig. 2B). The latter finding might indicate that endothelial cells with the higher levels of VEGFR-2 expression were more resistant to sunitinib than the rest of endothelial cells. Sunitinib treatment did not lead to the appearance of TUNEL-positive apoptotic cells in amounts corresponding to the decrease in CD31- or VEGFR-2–positive cells (Fig. 2B), most probably because of rapid shedding and clearance of the early-stage apoptotic tumor endothelial cells (*26*).

Increase in ^{99m}Tc-scVEGF Uptake After 3-Day Recovery from Sunitinib Treatment

Several groups reported revascularization of model and human tumors after the end of treatment with VEGF- and VEGFR-directed drugs (*25,27–29*). We tested if the earliest steps in this process were associated with enhanced VEGFR prevalence and therefore could be detected using ^{99m}Tc-scVEGF. A group of mice was treated with sunitinib

for 5 d and then allowed to recover for 3 d before imaging. Compared with after 1 d of recovery (Fig. 2A; Supplemental Fig. 5), after 3 d of recovery smaller differences existed in tumor size between treated and control mice as visualized by SPECT (Fig. 3A) or autoradiography (Fig. 3B). Despite the differences in sizes between tumors from treated and control mice, the enhanced tracer uptake at the edges of the tumors from recovered mice was clearly visible on all sections. As judged by the quantitative analysis of autoradiographs, a 3-d recovery period allowed for tracer accumulation in both rim and center to levels that were correspondingly 2.8-fold ($P = 0.0036$) and 1.5-fold ($P = 0.016$), respectively, higher than in a group with a 1-d recovery period (Fig. 3C).

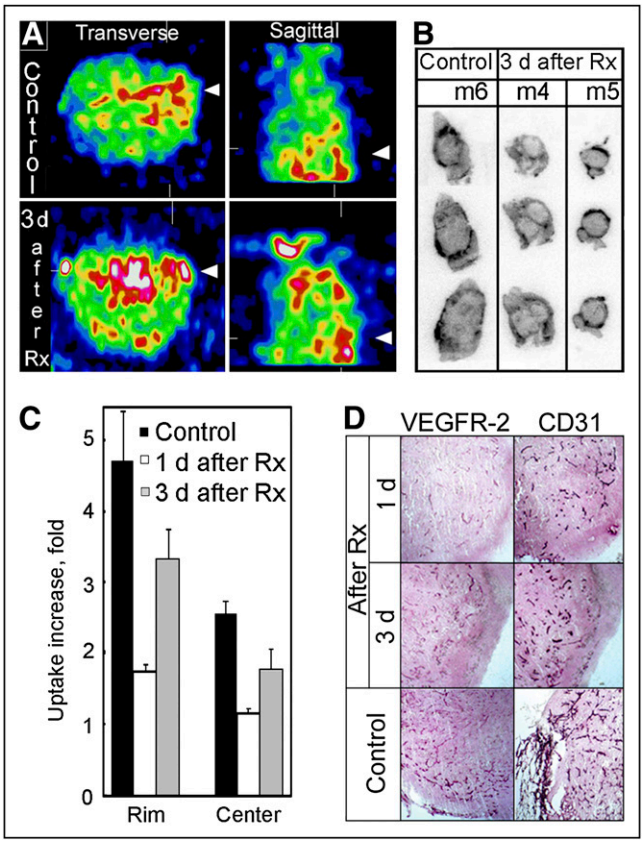

FIGURE 3. Enhanced ^{99m}Tc-scVEGF uptake and immunostaining for VEGFR-2 and CD31 after 4 d of sunitinib treatment and 3 d of recovery (3 d after treatment) relative to 1 d of recovery (1 d after treatment). (A) Representative SPECT image of treated and control MDA-231/luc tumor–bearing mice with ^{99m}Tc-scVEGF. Tomographic images are from center of tumors located in left axilla and left anterior chest wall. Standard of activity (capillary tube, 1 percentage injected dose per milliliter) is seen adjacent to right axilla. Arrowheads mark location of left axillary tumor. (B) Representative autoradiographs of serial 60-μm tumor sections of treated and control mice. (C) Quantitative analysis of autoradiographs. Increase in average radioactivity uptake per pixel relative to contralateral pectoral muscle was calculated using ImageQuant TL software. Differences between tracer uptake in control and treated animals after 1 d of recovery were statistically significant, with $P = 0.0001$ for both rim and center. Differences between tracer uptake in control and treated animals after 3 d of recovery were statistically significant, with $P = 0.009$ for rim and $P = 0.004$ for center. Differences between 1-d and 3-d recovery were statistically significant, with $P = 0.0036$ for rim and $P = 0.016$ for center. (D) VEGFR-2 and CD31 immunostaining, ×4 objective. m = mouse. Rx = treatment.

Immunohistochemical analysis of VEGFR-2 and CD31 in tumors harvested from imaged mice revealed higher levels of both markers after 3 d of recovery relative to 1 d of recovery (Fig. 3D). Notably, at the recovery stage, most VEGFR-2 and CD31 immunostaining was observed at the periphery of the tumor (Fig. 3D). In a separate group of mice both the decline and the recovery of VEGFR-2 and CD31 were characterized in more detail. As judged by quantitative analysis of immunostaining, both VEGFR-2 and CD31 declined rapidly from the beginning of treatment and then recovered as rapidly when the treatment was stopped (Figs. 4A and 4B; Supplemental Fig. 7).

Imaging Effects of 2 Weekly Cycles of Sunitinib

In clinical practice, sunitinib and other VEGFR inhibitors are usually given in several cycles. In the initial assessment of a 2-cycle treatment, 5 mice were treated with sunitinib for 5 d, given 2 d of rest, and treated again for 5 d. Then 2 mice were imaged after 1 d and 3 mice after 3 d of recovery. Judging by SPECT with ^{99m}Tc-scVEGF, after both 1 and 3 d of recovery there were mice with high and low levels of tracer uptake (Fig. 5A for 3-d recovery). The difference in tracer uptake was confirmed by autoradiography of serial sections of corresponding tumors (Fig. 5B). Tumors with high uptake (1 after 1 d of recovery and 2 after 3 d of recovery) had tracer uptakes similar to those of untreated controls (2 mice for each group). These preliminary data suggest that, at least in some mice, the sensitivity of tumor endothelium to sunitinib might be significantly decreased after 2 cycles of weekly treatment.

DISCUSSION

We report here that the early changes in VEGFR-2 prevalence in tumor vasculature induced either by treatment with sunitinib or by cessation of such treatment can be readily detected using noninvasive SPECT with ^{99m}Tc-scVEGF. After 4 daily 80 mg/kg doses of sunitinib and 1 d of recovery, the VEGFR-2 mediated uptake of ^{99m}Tc-scVEGF in tumor vasculature decreased 2.6- and 2.2-fold in the tumor rim and center, respectively (Figs. 2A and 3D). Because tissue culture experiments indicated that sunitinib does not prevent scVEGF-based tracer uptake (Fig. 1; Supplemental Figs. 2 and 3), the in vivo effects on tracer uptake could be attributed either to changes in VEGFR-2 prevalence or to changes in VEGFR-2 internalization and recycling. Immunohistochemical analysis of VEGFR-2 and CD31 expression in our tumor model indicated that 4 d of sunitinib treatment led to a significant decline in the number of VEGFR-2– and CD31-positive cells in tumor

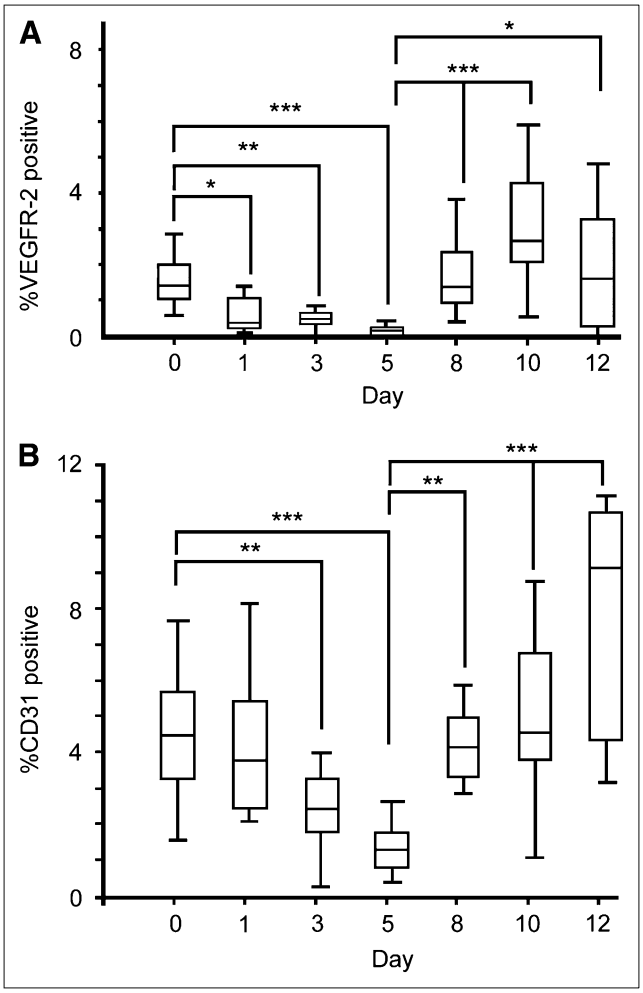

FIGURE 4. Sunitinib-induced decline in VEGFR-2 and CD31 immunostaining and rapid posttreatment recovery of vascularization at tumor edge. (A and B) Quantitative analysis of immunostaining for VEGFR-2 and CD31 (representative fields are shown in Supplemental Fig. 7) and percentage of pixels positive for, respectively, VEGFR-2 and CD31 immunostaining in 3–10 rectangular fields per section, obtained from 2–3 mice. Boxes represent interquartile region where middle 50% of data points occur, error bars represent minimum and maximum values in each group, and lines show median of each group. Comparisons between groups are indicated by brackets, and significance was determined by applying Kruskal–Wallis *Z* test with Bonferroni adjustment for multiple comparisons. $^{*}P < 0.05$. $^{**}P < 0.01$. $^{***}P < 0.001$.

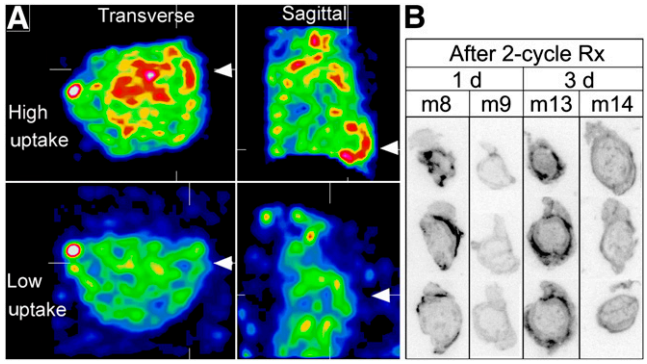

FIGURE 5. Two-cycle sunitinib treatment results in tumors with high and low levels of tracer uptake at 1 and 3 d after treatment. (A) SPECT of representative treated MDA-231/luc tumor–bearing mice with high and low levels of ^{99m}Tc-scVEGF uptake after the following protocol: 5 d treatment plus 2 d recovery plus 5 d treatment plus imaging 3 d after treatment. Tomographic images are from center of tumors located in left axilla and left anterior chest wall. Standard of activity (capillary tube, 1 percentage injected dose per milliliter) is seen adjacent to right axilla. Arrowheads mark location of left axillary tumor. (B) Autoradiographs of serial 60-μm tumor sections from 2 cycles of treatment plus imaging 1 or 3 d after treatment. Rx = treatment; m = mouse.

vasculature at the center and edge areas of the tumor (Figs. 2B and 4). Therefore, an approximately 2.5-fold decline in VEGFR-2 prevalence is primarily responsible for the 2.6- and 2.2-fold decline in ^{99m}Tc-scVEGF uptake. These data are in agreement with recent reports on a dramatic and rapid decrease in CD31-positive endothelial cells induced by various VEGF- and VEGFR-targeting drugs, including sunitinib (*19–24*). However, a more detailed and quantitative analysis would be necessary to establish a contribution of the changes in VEGFR-2 internalization and recycling into a decline in ^{99m}Tc-scVEGF uptake. This is particularly important in view of findings that VEGFR inhibitors affect VEGFR-2 recycling (*13*) and that the changes in VEGFR recycling induced by low concentrations of arginine-glycine-aspartic acid–mimetic integrin inhibitors might stimulate tumor growth and angiogenesis (*30*).

Currently, it is not clear how VEGFR-2– and CD31-positive tumor endothelial cells are affected by any 1 of the 3 main processes influenced by VEGFR-targeting drugs—namely, VEGF and VEGFR signaling in tumor endothelial cells, inhibition of signaling via other tyrosine kinase receptors, and systemic responses associated with inhibition of VEGF and VEGFR signaling in normal endothelium (*6*). Because VEGFR-targeting drugs do not eliminate normal endothelial cells, it is tempting to speculate that only tumor cells, but not normal endothelial cells, are addicted to VEGF and VEGFR signaling, for example, for activation of the PI3K/Akt survival pathway (*31*), in the same sense as was proposed for tumor cell addiction to oncogene-controlled signaling (*32*). For such addicted cells, blocking only 1 pathway might lead to cell death before alternative pathways are activated.

Once sunitinib treatment is discontinued, the decline in ^{99m}Tc-scVEGF uptake is reversed in as early as 3 d of recovery, as judged by SPECT and autoradiography. Immunohistochemical analysis revealed the rapid reestablishment of a dense vascular network, particularly at the tumor edges. Recovery of endothelial cells after treatment with VEGF- and VEGFR-targeting drugs was observed in mouse tumor models and in the clinic (*25,27–29*) and was recently

implicated in enhanced tumor invasiveness and metastatic dissemination (*33,34*). On the other hand, such recovery might provide for better access of chemotherapeutic agents to tumor cells, particularly at the growing tumor edge, where revascularization is significantly more prominent than in the central tumor region, supporting combination therapy with the schedule that takes into account the time of vascular recovery (*35*).

Our initial assessment of a longer 2-cycle treatment with sunitinib suggests that tumor endothelial cells in some mice became resistant to sunitinib, allowing for the reestablishment of a vascular network at the tumor edges. Revascularization of pancreatic islet tumors after several week of treatment with VEGFR-2–neutralizing antibody DC101 was reported previously (*36*). We have also observed revascularization at the tumor edges in HT29 tumors in mice treated for 2 wk with the VEGFR inhibitor pazopanib (*18*). Thus, it appears that tumor endothelium that arises from the host vasculature after prolonged treatment with different VEGF- and VEGFR-targeting drugs can expand despite continuous treatment with VEGFR-targeting drugs. Although such resistance might depend on multiple mechanisms (*37,38*), it is tempting to speculate that tumor endothelium that reemerges from the drug-resistant host vasculature that is resistant to VEGF- and VEGFR-targeting drugs is cured from the addiction to VEGF and VEGFR signaling and can engage alternative survival mechanisms.

Judging by the correlation between SPECT and autoradiography and immunohistochemical data, VEGFR-2 imaging with ^{99m}Tc-scVEGF detects both rapid collapse of tumor vasculature and resurgence of revascularized areas. What is important is that, unlike dynamic contrast-enhanced MRI, imaging of VEGFR-2 during the course of sunitinib treatment provides information on changes in the prevalence of the drug target, rather than on downstream effects, such as changes in perfusion. A recent report (*39*) on the lack of spatial correlation between dynamic contrast-enhanced MRI–based perfusion maps and VEGFR-2 distribution maps obtained with VEGFR-2–targeted ultrasound microbubbles supports the need for the direct assessment of VEGFR-2 prevalence. Although the clinical relevance and predictive value of the VEGFR-2 imaging can be ascertained only in clinical trials (*40*), we expect that it would be useful for direct surveillance and evaluation of VEGFR responses to VEGF- and VEGFR-directed therapies.

CONCLUSION

Our data indicate that SPECT of VEGFR with ^{99m}Tc-scVEGF detects both the initial decline and the following resurgence of VEGFR in tumor endothelium in the course of treatment with the small-molecule VEGFR inhibitor sunitinib. We expect that this approach can be expanded for monitoring dynamic changes of VEGFR in response to therapy with other tyrosine kinase inhibitors alone or in combination regimens and in response to therapy with bevacizumab using the bevacizumab-insensitive scVEGF(2GA)/^{99m}Tc tracer.

ACKNOWLEDGMENTS

We thank Yonaton S. Ray for his technical support in tissue culture experiments. This work was supported by NIH grants EB000898, EB006679, and CA113080. Joseph M. Backer is a shareholder in SibTech, Inc.

REFERENCES

1. Jubb AM, Oates AJ, Holden S, Koeppen H. Predicting benefit from antiangiogenic agents in malignancy. *Nat Rev Cancer.* 2006;6:626–635.
2. Lin MI, Sessa WC. Antiangiogenic therapy: creating a unique "window" of opportunity. *Cancer Cell.* 2004;6:529–531.
3. Jain RK, Duda DG, Clark JW, Loeffler JS. Lessons from phase III clinical trials on anti-VEGF therapy for cancer. *Nat Clin Pract Oncol.* 2006;3:24–40.
4. Ellis LM, Hicklin DJ. VEGF-targeted therapy: mechanisms of anti-tumour activity. *Nat Rev Cancer.* 2008;8:579–591.
5. Bergers G, Hanahan D. Modes of resistance to antiangiogenic therapy. *Nat Rev Cancer.* 2008;8:592–603.
6. Ebos JML, Lee CR, Kerbel RS. Tumor and host-mediated pathways of resistance and disease progression in response to antiangiogenic therapy. *Clin Cancer Res.* 2009;15:5020–5025.
7. Dempke WC, Heinemann V. Resistance to EGF-R (erbB-1) and VEGF-R modulating agents. *Eur J Cancer.* 2009;45:1117–1128.
8. Sessa C, Guibal A, Del Conte G, Ruegg C. Biomarkers of angiogenesis for the development of antiangiogenic therapies in oncology: tools or decorations? *Nat Clin Pract Oncol.* 2008;5:378–391.
9. Backer MV, Levashova Z, Patel V, et al. Molecular imaging of VEGF receptors in angiogenic vasculature with single-chain VEGF based probes. *Nat Med.* 2007; 13:504–509.
10. Levashova Z, Backer M, Backer JM, Blankenberg FG. Direct labeling of Cys-tag in scVEGF with technetium 99m. *Bioconjug Chem.* 2008;19:1049–1054.
11. Mendel DB, Laird AD, Xin X, et al. In vivo antitumor activity of SU11248, a novel tyrosine kinase inhibitor targeting vascular endothelial growth factor and platelet-derived growth factor receptors: determination of a pharmacokinetic/ pharmacodynamic relationship. *Clin Cancer Res.* 2003;9:327–337.
12. Levashova Z, Backer MV, Horng G, et al. SPECT and PET imaging of EGF receptor with site-specifically labeled EGF and dimeric EGF. *Bioconjug Chem.* 2009;20:742–749.
13. Ewan LC, Jopling HM, Jia H, et al. Intrinsic tyrosine kinase activity is required for vascular endothelial growth factor receptor 2 ubiquitination, sorting and degradation in endothelial cells. *Traffic.* 2006;7:1270–1282.
14. Dougher M, Terman BI. Autophosphorylation of KDR in the kinase domain is required for maximal VEGF-stimulated kinase activity and receptor internalization. *Oncogene.* 1999;18:1619–1627.
15. Santos SC, Miguel C, Domingues I, et al. VEGF and VEGFR-2 (KDR) internalization is required for endothelial recovery during wound healing. *Exp Cell Res.* 2007;313:1561–1574.
16. Fuh G, Wu P, Liang WC, et al. Structure-function studies of two synthetic anti-vascular endothelial growth factor Fabs and comparison with the Avastin Fab. *J Biol Chem.* 2006;281:6625–6631.
17. Sloan B, Scheinfeld NS. Pazopnib, a VEGF receptor tyrosine kinase inhibitor for cancer therapy. *Curr Opin Investig Drugs.* 2008;9:1324–1335.
18. Blankenberg FG, Levashova L, Sarkar SK, Pizzonia J, Backer MV, Backer JB. Noninvasive assessment of tumor VEGF receptors in response to treatment with pazopanib: a molecular imaging study. *Transl Oncol.* 2010;3:56–64.
19. Franco M, Man S, Chen L, et al. Targeted anti-vascular endothelial growth factor receptor-2 therapy leads to short-term and long-term impairment of vascular function and increase in tumor hypoxia. *Cancer Res.* 2006;66:3639–3648.
20. Palmowski M, Huppert J, Hauff P, et al. Vessel fractions in tumor xenografts depicted by flow- or contrast-sensitive three-dimensional high-frequency Doppler ultrasound respond differently to antiangiogenic treatment. *Cancer Res.* 2008;68:7042–7049.
21. Chang YS, Adnane J, Trail PA, et al. Sorafenib (BAY 43-9006) inhibits tumor growth and vascularization and induces tumor apoptosis and hypoxia in RCC xenograft models. *Cancer Chemother Pharmacol.* 2007;59:561–574.

22. Bozec A, Gros FX, Penault-Llorca F, et al. Vertical VEGF targeting: a combination of ligand blockade with receptor tyrosine kinase inhibition. *Eur J Cancer.* 2008;44:1922–1930.
23. Selvakumaran M, Yao KS, Feldman MD, O'Dwyer PJ. Antitumor effect of the angiogenesis inhibitor bevacizumab is dependent on susceptibility of tumors to hypoxia-induced apoptosis. *Biochem Pharmacol.* 2008;75:627–668.
24. Smith NR, James NH, Oakley I, et al. Acute pharmacodynamic and antivascular effects of the vascular endothelial growth factor signaling inhibitor AZD2171 in Calu-6 human lung tumor xenografts. *Mol Cancer Ther.* 2007;6:2198–2208.
25. Christensen JG. A preclinical review of sunitinib, a multitargeted receptor tyrosine kinase inhibitor with anti-angiogenic and antitumour activities. *Ann Oncol.* 2007;18(suppl 10):x3–x10.
26. Benjamin LE, Keshet E. Conditional switching of vascular endothelial growth factor (VEGF) expression in tumors: induction of endothelial cell shedding and regression of hemangioblastoma-like vessels by VEGF withdrawal. *Proc Natl Acad Sci USA.* 1997;94:8761–8766.
27. Mancuso MR, Davis R, Norberg SM. Rapid vascular regrowth in tumors after reversal of VEGF inhibition. *J Clin Invest.* 2006;116:2610–2621.
28. Burstein HJ, Elias AD, Rugo HS, et al. Phase II study of sunitinib malate, an oral multitargeted tyrosine kinase inhibitor, in patients with metastatic breast cancer previously treated with an anthracycline and a taxane. *J Clin Oncol.* 2008;26: 1810–1816.
29. Johannsen M, Flörcken A, Bex A, et al. Can tyrosine kinase inhibitors be discontinued in patients with metastatic renal cell carcinoma and a complete response to treatment? A multicentre, retrospective analysis. *Eur Urol.* 2009;55:1430–1438.
30. Reynolds AR, Hart IR, Watson AR, et al. Stimulation of tumor growth and angiogenesis by low concentrations of RGD-mimetic integrin inhibitors. *Nat Med.* 2009;15:392–400.
31. Sakamaki K. Regulation of endothelial cell death and its role in angiogenesis and vascular regression. *Curr Neurovasc Res.* 2004;1:305–315.
32. Weinstein IB, Joe AK. Oncogene addiction. *Cancer Res.* 2008;68:3077–3080.
33. Paez-Ribes M, Allen E, Hudock J, et al. Antiangiogenic therapy elicits malignant progression of tumors to increased local invasion and distant metastasis. *Cancer Cell.* 2009;15:220–231.
34. Ebos JM, Lee CR, Cruz-Munoz W, Bjarnason GA, Christensen JG, Kerbel RS. Accelerated metastasis after short-term treatment with a potent inhibitor of tumor angiogenesis. *Cancer Cell.* 2009;15:232–239.
35. Kerbel RS, Kamen BA. The anti-angiogenesis basis of metronomic chemotherapy. *Nat Rev Cancer.* 2004;4:423–436.
36. Casanovas O, Hicklin DJ, Bergers G, Hanahan D. Drug resistance by evasion of antiangiogenic targeting of VEGF signaling in late-stage pancreatic islet tumors. *Cancer Cell.* 2005;8:299–309.
37. Xiong YQ, Sun HC, Zhang W, et al. Human hepatocellular carcinoma tumor–derived endothelial cells manifest increased angiogenesis capability and drug resistance compared with normal endothelial cells. *Clin Cancer Res.* 2009;15: 4838–4846.
38. Dudley AC, Klagsbrun M. Tumor endothelial cells join the resistance. *Clin Cancer Res.* 2009;15:4787–4789.
39. Loveless ME, Whisenant JG, Wilson K, et al. Coregistration of ultrasonography and magnetic resonance imaging with a preliminary investigation of the spatial colocalization of vascular endothelial growth factor receptor 2 expression and tumor perfusion in a murine tumor model. *Mol Imaging.* 2009;8:187–198.
40. Sargent DJ, Rubinstein L, Schwartz L, et al. Validation of novel imaging methodologies for use as cancer clinical trial end-points. *Eur J Cancer.* 2009;45: 290–299.